PERGAMON

Available online at www.sciencedirect.com

SCIENCE DIRECT®

Corrosion Science 45 (2003) 2163–2175

CORROSION SCIENCE

www.elsevier.com/locate/corsci

Corrosion protection of AA 2024-T3 by bis-[3-(triethoxysilyl)propyl]tetrasulfide in neutral sodium chloride solution. Part 1: corrosion of AA 2024-T3

Danqing Zhu, Wim J. van Ooij *

Department of Materials Science and Engineering, University of Cincinnati, P.O. Box 210012, Cincinnati, OH 45221-0012, USA

Received 8 March 2002; accepted 21 February 2003

Abstract

This study consists of two parts. In the first part, the corrosion of 2024-T3 aluminum alloy (AA 2024-T3) was studied using scanning electron microscopy and energy-dispersive X-ray spectroscopy. The results showed that the anodic S phase (Al_2CuMg) particles dealloyed Al and Mg during the 3.5 h of immersion in a neutral 0.6 M sodium chloride (NaCl) solution; with the dealloying of Mg being the most severe. Simultaneously, a heavy dissolution was also observed for the surrounding Al matrix of the S phase particles. This Al dissolution is likely to be caused by a local alkalization resulting from the coupled cathodic reaction (water and/or oxygen reduction). Such corrosion in AA 2024-T3, however, can be inhibited efficiently after the treatment of bis-[3-(triethoxysilyl)propyl]tetrasulfide (bis-sulfur silane). The associated studies on bis-sulfur silane treated AA 2024-T3 will be presented in the second part.

Keywords: AA 2024-T3; B. SEM; Pitting; Cathodic corrosion

1. Introduction

The 2024-T3 aluminum alloy (AA 2024-T3) is extensively used in aerospace industries due to its excellent mechanical properties. Such mechanical properties are

* Corresponding author. Tel.: +1-513-556-3194; fax: +1-513-556-3773.
E-mail address: vanooiwj@email.uc.edu (W.J. van Ooij).

0010-938X/03/$ - see front matter © 2003 Elsevier Ltd. All rights reserved.
doi:10.1016/S0010-938X(03)00060-X

achieved by the strengthening of the alloy matrix with a number of second-phase particles. Some particles, however, are not desirable from a corrosion prevention perspective. The anodic S phase particles (Al_2CuMg), for example, cause severe pitting of the alloy when exposed to a chloride-containing environment [1–4]. Chromating processes, such as the Alodine® process, are therefore used as an anticorrosive surface treatment for AA 2024-T3.

Recently, the use of chromating has been heavily restricted by environmental legislations due to the high toxicity and carcinogenity of hexavalent chromium ions (Cr(VI)). A need for an alternative anticorrosion surface treatment has thus evolved. Various inorganic and organic corrosion inhibitors have been proposed and studied. Among them, silane surface treatment is a promising alternative that has attracted a lot of attention from industries in the recent years. In general, this technology includes attractive benefits such as environmental compliance, economical application, and good corrosion inhibition as well as paint adhesion to a variety of metals.

Before extending the study of clarifying the roles of silanes playing in the corrosion protection of AA 2024-T3, the corrosion behavior of bare AA 2024-T3 during immersion in a neutral NaCl solution was studied, and the results are reported here. The second part of the report involved the investigation of the anticorrosion mechanism of bis-sulfur silane-treated AA 2024-T3 system using a variety of electrochemical tests. From these test results, a mechanism for the corrosion inhibition of AA 2024-T3 by silanes is presented.

2. Experimental

2.1. Materials

AA 2024-T3 panels with the dimension of 10 cm × 15 cm × 0.06 cm (width × length × thickness) were purchased from ACT Inc. (Hillsdale, MI). The AA 2024-T3 panels were cut into coupons with dimensions of 2.5 cm × 2.5 cm, polished mechanically using SiC polishing papers with different grades, and finished with a 5-μm alumina paste. The polished mirror-like surfaces were then cleaned ultrasonically for 5 min in ethanol.

2.2. Immersion test

A polished AA 2024-T3 coupon was immersed in a 0.6 M NaCl aqueous solution at pH 6.5 for various times to initiate pitting in AA 2024-T3. The alloy surface was examined using scanning electron microscopy (SEM) and energy-dispersive X-ray spectrometry (EDX) before and after the test.

2.3. SEM/EDX

Surface observations were conducted using a Hitachi S4000 SEM, equipped with an EDX spectrometer. The accelerating voltage was 20 kV.

3. Results

3.1. Identification of second-phase particles in AA 2024-T3

Fig. 1 shows a uniform distribution of the second-phase particles in the matrix of AA 2024-T3. This area was randomly chosen on a freshly polished alloy surface. These particles serve to strengthen the alloy matrix giving it excellent mechanical properties. However, anodic S phase particles lead to a poor corrosion performance of the alloy [1–4]. According to the literature [1–4], two major groups of second-phase particles are observed frequently in AA 2024-T3: one is Al–Cu–Mg-containing (or Al_2CuMg, S phase) particles and the other is Al–Cu–Fe–Mn-containing particles. The former is anodic towards the Al matrix and the latter is cathodic with respect to the Al matrix.

By examining the alloy studied in this work, we found 4 types of second-phase particles with different chemical compositions: Al–Cu–Mg-containing (S phase), Al–Cu–Fe–Mn–Si-containing, Al–Si-containing, and Al–Cu-containing (θ phase). It is noted that the latter two are seldom observed in the literature [1–4]. The corresponding SEM images of these particles are shown in Fig. 2(a)–(d). Both S and θ have a round shape (Fig. 2(a) and (d)), while the other two are much more irregular-shaped (Fig. 2(b) and (c)). The chemical compositions of these particles were determined by EDX and are listed in Table 1. On the average, 4 particles of each kind (>1 μm) were examined. Only the S phase contains a high amount of Mg, about 14 at.%.

3.2. SEM/EDX observation of corrosion of AA 2024-T3 during immersion in a neutral NaCl solution

Before immersion, an arbitrary area on the polished alloy surface was selected, as shown in Fig. 3(a). The compositions of some of the large particles were identified

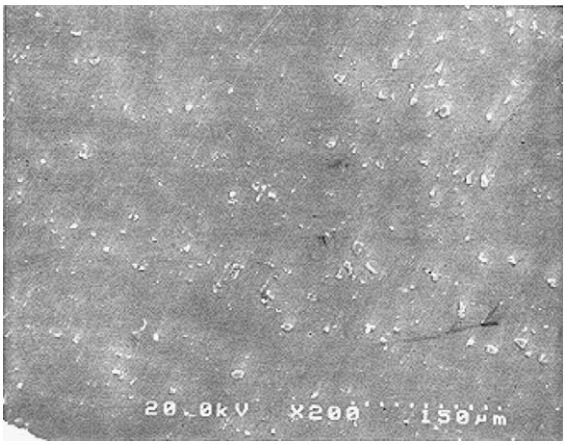

Fig. 1. Distribution of second-phase particles in the matrix of AA 2024-T3.

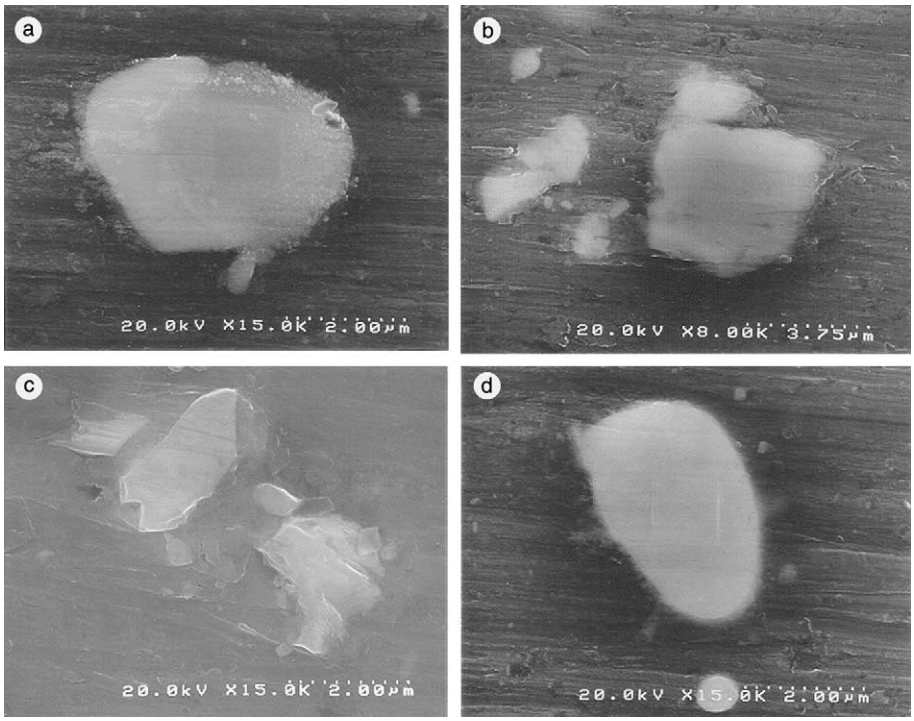

Fig. 2. SEM images and the corresponding EDX spectra of second-phase particles in AA 2024-T3; (a) Al–Cu–Mg-containing, (b) Al–Cu–Fe–Mn–Si-containing, (c) Al–Si-containing, and (d) Al–Cu-containing.

Table 1
Chemical composition (in at.%) of second-phase particles in AA 2024-T3

Element	Al–Cu–Mg-containing	Al–Cu–Fe–Mn-containing	Al–Si-containing	Al–Cu-containing
Al	76.4	77.1	27.3	75.2
Cu	13.4	6.8	–	24.8
Mg	10.2	–	–	–
Fe	–	8.5	–	–
Mn	–	4.8	–	–
Si	–	2.7	72.1	–

with SEM/EDX. The particles marked as "A_1" and "A_2" contain Al–Cu–Mg and are designated as S phase; those labeled as "B_1" and "B_2" contain Al–Cu–Fe–Mn–Si; and the particles "C_1" and "C_2" contain Al–Si. θ phase particles were not detected in this area. This may be due to their low area fraction.

The polished coupon was immersed into a stagnant 0.6 M NaCl aqueous solution (pH 6.5). The solution was open to air throughout the entire test period. During the immersion, the alloy surface was found to corrode gradually. After 3.5 h, the coupon was taken out and rinsed with tap water. The same area shown in Fig. 3(a) was re-examined with SEM/EDX, as shown in Fig. 3(b). It is seen that only the regions

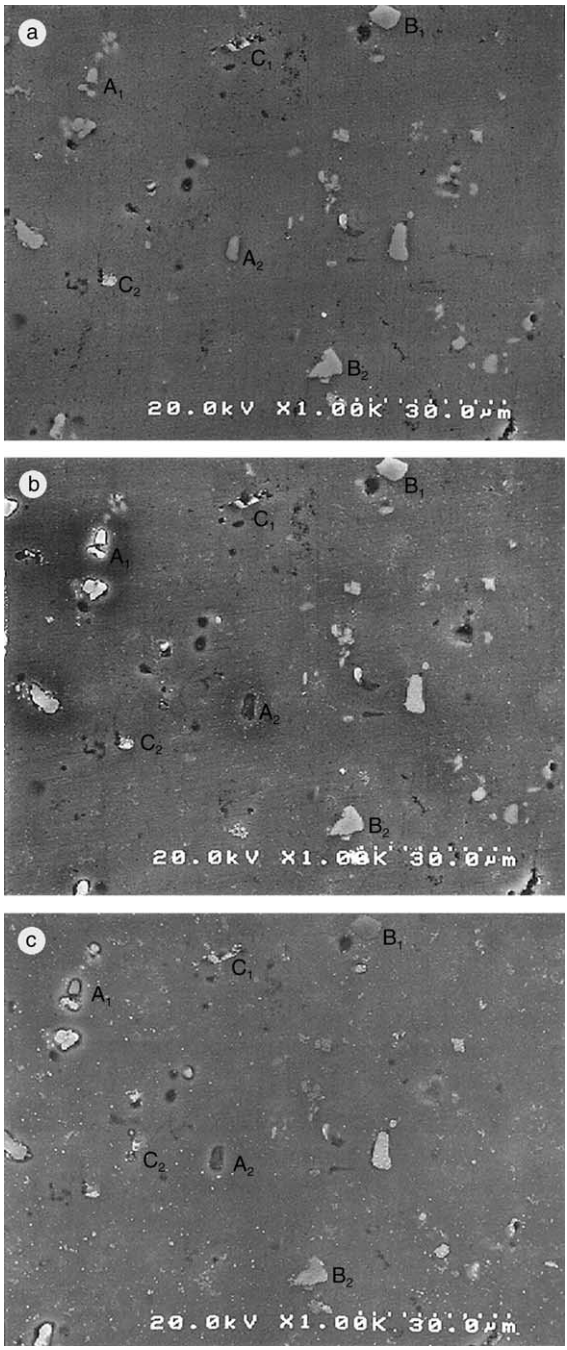

Fig. 3. SEM images of the AA 2024-T3 sample immersed in a neutral 0.6 M NaCl solution; (a) before immersion, (b) after 3.5 h of immersion, and (c) after 72 h of immersion.

around the S phase particles (i.e., A_1 and A_2) corroded heavily. The Al matrix around the S phase particles at site A_1 dissolved substantially; while the S phase particle at A_2 fell out or decomposed into nano-particles spreading over the pit edge. No corrosion is actually visible in the vicinities of particles B_1, B_2, C_1 and C_2. This observation indicates that the onset of pitting corrosion of AA 2024-T3 is indeed associated with the S phase particles. After the SEM observation, the sample was then re-immersed into the NaCl solution until the end of the test, i.e., 72 h of immersion. Fig. 3(c) shows the SEM image of the sample surface corresponding to after 72 h of immersion. The alloy surface is similar to that shown in Fig. 3(b), except that a large quantity of nano-particles are distributed uniformly all over the surface.

Fig. 4 shows the changes in the composition of the S phase particle located at site A_1 as a function of immersion time. In Fig. 4, the contents of both Al and Mg are seen to decrease continuously during immersion. The atomic percent of Mg drops sharply from 15.4% to 1.3% in the first 3.5 h, and continuously decreases to 0.9% after 72 h. The percent of Al also decreases to some extent, from 65.6% to 58.1% after 72 h. The Cu content in the remnant, however, remains almost constant at around 19.0% in the first 3.5 h, and increases slightly up to 21.4% after 72 h. These changes indicate that the S phase particle experienced dealloying of Mg and Al during immersion, with the dealloying of Mg being the most severe in the first 3.5 h. As a result, a remnant enriched with Cu was left behind. 17.8% of O detected after testing is surely from the corrosion products. The SEM images of two adjacent S phase remnants at site A_1 corresponding to 3.5 and 72 h of immersion are presented in Fig. 5(a) and (b), where no significant changes in the pit morphology are observed after 72 h. This implies that severe pitting corrosion of AA 2024-T3 occurred mainly in the very early stages (e.g., 3.5 h), exhibiting as the dealloying of S phase and the dissolution of the surrounding Al matrix.

The particles labeled as B_1 (Al–Cu–Mn–Fe-containing) and C_1 (Al–Si-containing) in Fig. 3 are both cathodic towards the Al matrix [1–5]. After 3.5 h of immersion,

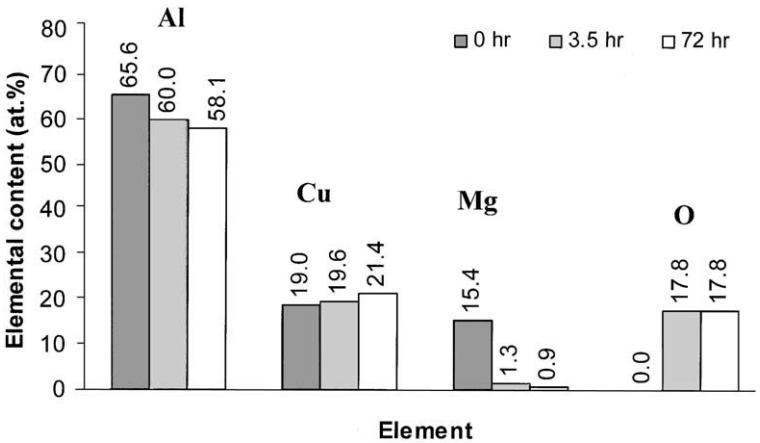

Fig. 4. Elemental compositions of the S phase particle at A_1 as a function of immersion time.

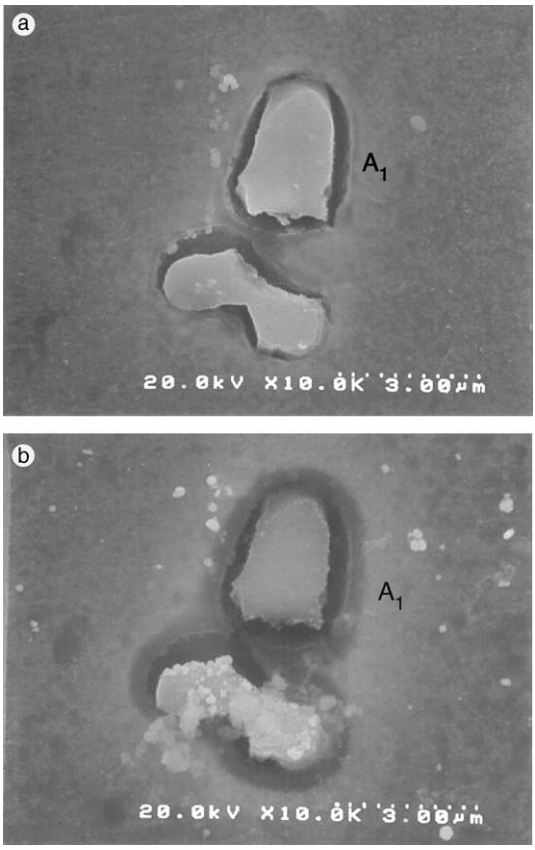

Fig. 5. SEM images of two adjacent S phase remnants at A_1 after immersion in a 0.6 M NaCl solution (pH 6.5) for various times; (a) 3.5 h, and (b) 72 h (note: the EDX in Fig. 4 results were obtained from the S phase remnant on the top).

these two particles and their surrounding Al matrix remained intact without showing any corrosion sign. Some noticeable morphological changes, however, are observed after 72 h of immersion, as displayed in Fig. 6(a) and (b). In Fig. 6(a), a micro-crack is seen along the Al–Cu–Mn–Fe-containing particle; moreover, nodular particles spread uniformly over the entire particle surface. This micro-crack possibly resulted from a slight anodic dissolution of the Al matrix. In Fig. 6(b), a similar distribution of nodular particles is seen on the Al–Si particle surface after 72 h. However, no micro-crack is observed along the Al–Si-containing particle.

Similar observation for nodular particles was also reported by others [2,4]. According to these studies [2,4], the nodular particles found on both cathodic second-phase particles are pure Cu. Chen et al. [2] stated that the Al–Cu–Mn–Fe-containing particles function as cathodic sites, which favors cupric ions (Cu^{2+}) dissolved in the NaCl solution to be reduced as nodular Cu deposits on the particles. Obispo et al. [4] studied Cu deposition on AA 2024-T3 by using TEM/EDX along with a

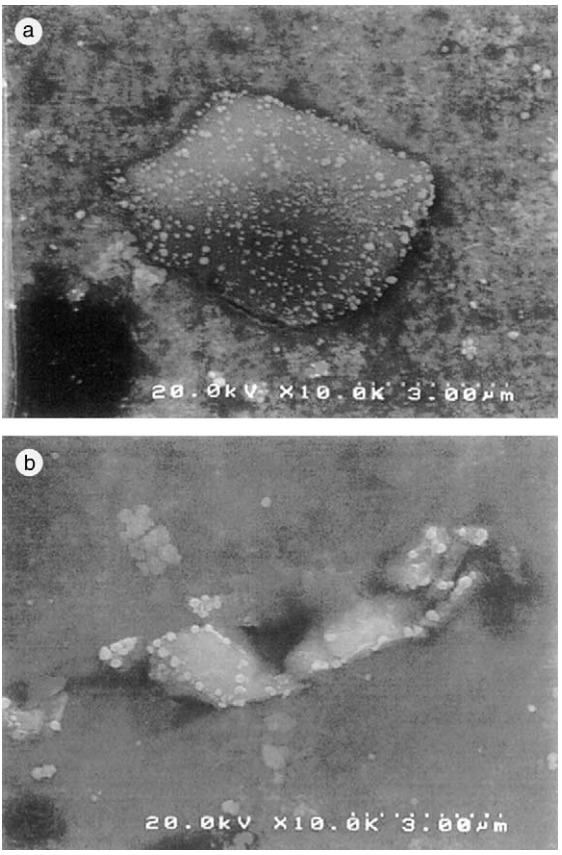

Fig. 6. SEM images of the cathodic particles after 72 h of immersion in a 0.6 M NaCl solution (pH 6.5); (a) Al–Cu–Fe–Mn-containing particle (at B_1 in Fig. 3), and (b) Al–Si-containing particle (at C_1 in Fig. 3).

replica-based lift-off technique to enhance the particle and surface debris resolution. They observed large Cu clusters deposited on Fe-rich or Fe-containing areas when AA 2024-T3 was immersed in NaCl solutions. They suggested that the reduction of copper from solution is an electrochemical displacement reaction which is very likely to occur on cathodic particles by oxidization or dealloying of electroactive elements such as iron (Fe) out of the particles. As might be noted in Fig. 5(b), a cluster of nodular particles are also displayed on the surface of the dealloyed S phase remnant (the bottom one). This might indicate that after dealloying to a certain extent, the S phase remnant becomes so cathodic towards the Al matrix that it turns into a favorable place for Cu reduction, as the other two cathodic particles do.

An alternative explanation given by Buchheit et al. [1] for the distribution of Cu nodular particles on the AA 2024-T3 surface is as follows. The appearance of these Cu nano-particles is most likely a result of the decomposition of porously structured Cu-rich remnants. The Cu-rich remnants decompose into nano-particles, and later

on they are transported away from the original sites by mechanical motion, spreading over the alloy surface.

4. Discussion

4.1. Pitting associated with anodic S phase particles in AA 2024-T3

The mechanism for pitting associated with S phase particles in AA 2024-T3 has been discussed earlier [1]. In summation, corrosion of AA 2024-T3 starts from the dealloying of anodic S phase particles as a result of galvanic corrosion driven by the galvanic couple of anodic S phase and cathodic Al matrix, which was also confirmed in this work.

As for the dissolution of the surrounding Al matrix along the S phase particles, the explanation in Ref. [1] is as follows. As dealloying continues, the S phase remnants become Cu-rich and finally turn into cathodes towards the adjacent Al matrix. Consequently, the opposite galvanic couple of anodic Al matrix and cathodic Cu-rich S phase remnant is established. This would lead to another galvanic corrosion, causing dissolution of the surrounding Al matrix [1]. However, this explanation is not fully supported by the experimental evidence in this work.

If the above explanation were the case, then we would have expected to observe a much more severe dissolution of Al matrix in the later stages (i.e., 72 h), as the S phase remnants would become more cathodic towards the surrounding Al matrix in the later stages due to the completion of the dealloying. As opposed with what was expected, the Al matrix around the S phase particles was only observed to dissolve heavily within the first 3.5 h (Fig. 5(a)) along with the dealloying of the S phase particles. Further dissolution of the Al matrix seemed to cease or to slow down in the later stages even when the S phase remnant became more cathodic towards the Al matrix (Fig. 5(b)). A question hence arises here: is the galvanic corrosion suggested in Ref. [1] the primary cause for the several Al dissolution around the S phase particles? In Section 4.3, we will further discuss this issue in consideration of some other possibilities.

4.2. Corrosion behavior of cathodic Al–Cu–Fe–Mn-containing and Al–Si-containing phase particles in AA 2024-T3

The other two cathodic particles (i.e., Al–Cu–Fe–Mn-containing and Al–Si-containing particles) did not corrode within the first 3.5 h (Fig. 3(b)). After 72 h, only a slight trench or a micro-crack was formed around the Al–Cu–Mn-containing particle (Fig. 6(a)), and no corrosion activity was seen in the vicinity of the Al–Si-containing particle (Fig. 6(b)). Al–Cu–Fe–Mn-containing phase, for example, has a corrosion potential of −0.35 V/SCE in chloride-containing solutions [6], 0.2 V/SCE positive towards AA 2024-T3 matrix (−0.65 V/SCE). In principle, a galvanic couple of anodic Al matrix/cathodic Al–Cu–Fe–Mn-containing phase should be developed, inducing the dissolution of the surrounding Al matrix. In reality, however, we did not observe

a severe dissolution of the Al matrix along the particle throughout immersion. This phenomenon is understandable by taking into account the effect of the cathode-to-anode area ratio on galvanic corrosion.

It is known that galvanic corrosion can either be accelerated by increasing the cathode-to-anode area ratio, or be weakened by reducing the ratio. In the former case, galvanic corrosion concentrates on a small anode, causing a severe damage of the anode. This actually explains the extensive dealloying of the anodic S phase particles in the first 3.5 h. The S phase particles as small anodes suffered intensive galvanic corrosion, as they were surrounded by the large cathodic Al matrix. In the latter case, the induced galvanic attack spreads over a greater anodic area. The corrosion activity on the anode is therefore weakened. This is exactly the case for these two cathodic particles. Compared to the surrounding Al matrix, these two cathodic particles are relatively small. The galvanic attack induced by these two small cathodic particles would readily spread over a large area of the anodic Al matrix. As a result, a severe dissolution of the Al matrix is avoided (Fig. 6(a) and (b)).

By the use of this area ratio effect, the corrosion behavior of the dealloyed S phase remnants in the later stages can also be explained. In the later stages, the dealloyed S phase remnants serve as small cathodes like the other two cathodic particles. Such small cathodic S phase remnants, however, are incapable of inducing a severe Al dissolution at the peripheries, due to the effect of the small cathode-to-anode area ratio.

4.3. Alternative mechanism of Al dissolution in the vicinity of S phase particles

As discussed in Section 4.1, the SEM/EDX observation in this work does not support the suggested mechanism for the severe dissolution of the Al matrix in the vicinity of the S phase remnants [1]. In this section, we give an alternative explanation to this phenomenon in consideration of some other possibilities.

Fig. 7 schematically shows pitting corrosion of AA 2024-T3 in a naturally aerated neutral chloride-containing solution. The overall corrosion starts with the dealloying of the anodic S phase particle. The corresponding anodic and cathodic reactions are given by

$$\text{Anodic reaction 1:}\quad \mathrm{Mg} \rightarrow \mathrm{Mg^{2+}} + 2\mathrm{e}\ \text{(dealloying of Mg)} \tag{1}$$

$$\text{Anodic reaction 2:}\quad \mathrm{Al} \rightarrow \mathrm{Al^{3+}} + 3\mathrm{e}\ \text{(dealloying of Al)} \tag{2}$$

and,

$$\text{Cathodic reaction 1:}\quad 2\mathrm{H_2O} + 2\mathrm{e} \rightarrow \mathrm{H_2}\uparrow + 2\mathrm{OH^-}\ \text{(water reduction)} \tag{3}$$

$$\text{Cathodic reaction 2:}\quad \mathrm{O_2} + 2\mathrm{H_2O} + 4\mathrm{e} \rightarrow 4\mathrm{OH^-}\ \text{(oxygen reduction)} \tag{4}$$

The above anodic reactions (i.e., dealloying of Mg and Al) occur at the surface of the S phase particles. The accompanying cathodic reactions, water reduction and oxygen reduction, are most likely to take place on the Al matrix at the periphery of the S phase particles. It should be noted that along with the S phase dealloying, the

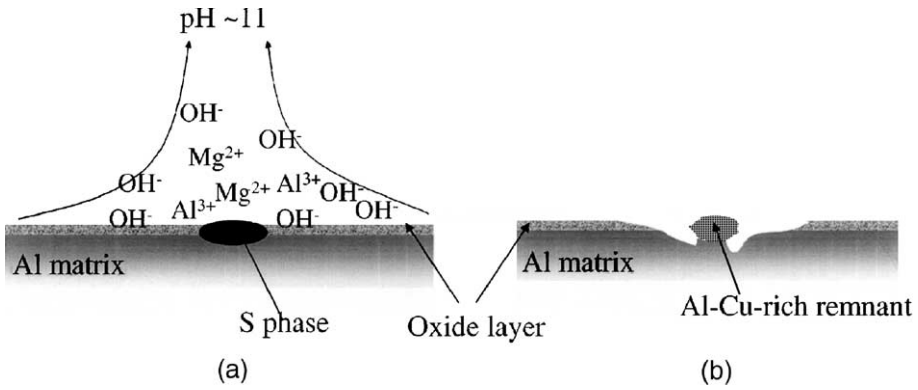

Fig. 7. Schematic of early corrosion of AA 2024-T3 in a neutral 0.6 M NaCl solution; (a) dealloying and local alkalization, and (b) cathodic corrosion of the surrounding Al matrix.

coupled cathodic reactions (3) and (4) would also generate hydroxide ions (OH^-) by reducing water and/or oxygen molecules. The rate of water reduction and the amount of OH^- ions is obviously determined by the rates and the extent of the anodic reactions (1) and (2). Since Mg was observed to dissolve significantly within 3.5 h from the S phase particles, it is reasonable to expect a considerably high amount of OH^- ions generated from the coupled water and oxygen reductions. Accordingly, a local alkalization is formed around the S phase remnant in a stagnant solution (Fig. 7(a)). Once the local pH exceeds 9 (i.e., the equilibrium pH of Al oxide), the surrounding Al oxide layer on the Al matrix would no longer survive and would dissolve according to

$$Al_2O_3 + 2OH^-(ad) \Longleftrightarrow 2AlO_2^-(aq) + H_2O \tag{5}$$

Simultaneously, the bare Al matrix underneath would be oxidized to form a new layer of Al oxide, releasing hydrogen gas by the reaction,

$$2Al(m) + 3H_2O \Longleftrightarrow Al_2O_3 + 3H_2\uparrow \tag{6}$$

where $OH^-(ad)$ = the adsorbed hydroxide ion; $AlO_2^-(aq)$ = the aluminate ion in the aqueous solution; Al(m) = the Al atom in the Al lattice. It should be noted that the dissolution of Al oxide (5) is simply a chemical dissolution (i.e., without electron transfer), whereas the formation of the Al oxide (6) is an electrochemical process in which an electron transfer (or metal oxidation) is involved [7]. The Al dissolution in an alkaline medium in Fig. 7(b) is also called "cathodic corrosion" of Al.

The local pH increase around the S phase particle may increase to 11 (i.e., the equilibrium pH of protective Mg oxide ($Mg(OH)_2$)), below which $Mg(OH)_2$ cannot be formed. In the presence of chloride ions (Cl^-), the formation of $Mg(OH)_2$ may be further delayed, as the Cl^- ions are known to de-stabilize $Mg(OH)_2$ [8].

A similar mechanism for corrosion of AA 5085 and AA 6061 in a neutral NaCl solution was proposed by Eleboujdaini and Ghali [9,10]. They stated that a high

content of electroactive Mg in the second-phases in both alloys increases the cathodic activity (i.e., hydrogen evolution at the Mg-rich particle surfaces). As a result, an alkaline diffusion layer located along the particles is formed, which leads to the dissolution of the matrix around the particles and final removal of Mg-rich particles from the surface. When the cathodic activity ceases, a protective oxide film is re-formed on the surface of the pit in place of the removed particle. Other similar works have also been documented [11–13].

In the case of AA 2024-T3, the corrosion of the Al matrix related to the dealloying of S phase is very likely the same. That is, the surrounding Al matrix undergoes cathodic corrosion caused by a high local pH environment, rather than galvanic corrosion driven by the opposite galvanic relationship developed between S phase remnants and the surrounding Al matrix stated in Ref. [1]. If the galvanic corrosion were the case, then a more severe dissolution of Al matrix would have been observed in the later stages of immersion, as the S phase remnant becomes more cathodic towards the surrounding Al matrix in the later stage due to the completion of the dealloying. However, such phenomenon was not observed in this work.

Based on our work and the discussion in the other literature [9–13], our conclusion is as follows. The Al matrix is most likely to experience a severe cathodic dissolution due to the local alkalization formed along the dealloying of S phase in the early stages. The overall cathodic dissolution of the surrounding Al matrix consists of the following two simultaneous processes: (1) chemical dissolution of the Al oxide layer; and (2) electrochemical formation of a new layer of Al oxide by the oxidation of the bare Al matrix.

5. Conclusions

The results of the corrosion study of AA 2024-T3 in a neutral NaCl solution showed that, (1) pitting initiates around the anodic S phase particles, exhibiting as the dealloying of elements Al and Mg and the severe dissolution of the surrounding Al matrix; (2) the Al dissolution in the vicinity of S phase remnants is likely to be caused by the local alkalization resulting from the coupled cathodic reactions (water/oxygen reduction), rather than by the galvanic corrosion induced by the galvanic couple of the Cu-rich S phase remnants (cathode) and the surrounding Al matrix (anode) [1]. Such corrosion, however, can be inhibited by a bis-sulfur silane treatment, as will be demonstrated in a separate paper of AA2024-T3.

Acknowledgements

The authors gratefully acknowledge the financial support for this work by the Air Force Office of Scientific Research under contract F49620-01-1-0352. We also wish to thank Dr. Niloy Mukherjee for SEM operation.

References

[1] R.G. Buchheit, R.P. Grant, P.F. Halva, B. Mckenie, G.L. Zender, J. Electrochem. Soc. 144 (8) (1997) 2621.
[2] G.S. Chen, M. Gao, R.P. Wei, Corrosion 52 (1) (1996) 8.
[3] V. Guillaumin, G. Mankowski, Corros. Sci. 41 (1990) 421.
[4] H.M. Obispo, L.E. Murr, M. Arrowood, E.A. Trillo, J. Mater. Sci. 35 (2000) 3479.
[5] R.G. Buchheit, J. Electrochem. Soc. 142 (1995) 3994.
[6] G.O. Ilevbare, J.R. Scully, Corrosion 57 (2001) 134.
[7] S.-M. Moon, S.-I. Pyun, Corros. Sci. 39 (2) (1997) 399.
[8] E. Ghali, Magnesium and magnesium alloys, in: R.W. Revie (Ed.), Uhlig's Corrosion Handbook, second ed., John Wiley & Son, Inc., New York, 2000, p. 793.
[9] M. Eleboujdaini, E. Ghali, Electrochim. Acta (1992) 412.
[10] M. Eleboujdaini, E. Ghali, R.G. Barrada, M. Firgis, Corros. Sci. 30 (1990) 855.
[11] K. Nisancioglu, K.Y. Davanger, O. Strandmylr, J. Electrochem. Soc. 127 (1980) 1325.
[12] K. Nisancioglu, O. Lunder, H. Holtan, Corrosion 41 (1985) 247.
[13] B. Mazurkiewicz, Corros. Sci. 23 (1983) 687.